J|A|C|S
ARTICLES

Published on Web 11/18/2009

# Luminescent Ethynyl−Pyrene Liquid Crystals and Gels for Optoelectronic Devices

Stéphane Diring,[†] Franck Camerel,[†] Bertrand Donnio,[‡] Thierry Dintzer,[§] Stefano Toffanin,[||] Raffaella Capelli,[||] Michele Muccini,*[,||] and Raymond Ziessel*[,†]

*Laboratoire de Chimie Organique et Spectroscopies Avancées (LCOSA), UMR 7515, CNRS-ECPM, Université de Strasbourg, 25 Rue Becquerel, 67087 Strasbourg Cedex 2, France, Institut de Physique et Chimie des Matériaux de Strasbourg (IPCMS), UMR 7504, CNRS-Université de Strasbourg, 23 rue du Loess, BP 43, 67034 Strasbourg Cedex 2, France, Laboratoire des Matériaux, Surface et Procédés pour la Catalyse (LMSPC), UMR 7515, CNRS-ECPM, Université de Strasbourg, 25 rue Becquerel, 67087 Strasbourg Cedex 2, France, and Consiglio Nazionale delle Ricerche (CNR), Istituto per lo Studio dei Materiali Nanostrutturati (ISMN), via P. Gobetti 101, I-40129 Bologna, Italy*

Received September 22, 2009; E-mail: ziessel@unistra.fr; m.muccini@bo.ismn.cnr.it

***Abstract:*** Two functional ethynyl−pyrene derivatives have been designed and synthesized by di- and tetra-substitutions of bromo pyrene derivatives with *N*-(4-ethynylphenyl)-3,4,5-tris(hexadecyloxy)benzamide fragments. The photoluminescence wavelength of the pyrene core can be tuned by the substitution pattern and the state of matter (solid, solution, gel, or liquid crystal). The disubstituted pyrene derivative **1** is not mesomorphic but produces robust and highly fluorescent gels in DMF, toluene, and cyclohexane. The well-defined fibers and ropes of the gel states were characterized by SEM and laser scanning confocal microscopy, and extended over several micrometers. The gels were integrated as active layers in field-effect transistors, which provided good bulk electron and hole charge mobilities as well as light emission generation. The tetra-substituted pyrene derivative is not a gelator but displays a stable liquid crystalline phase with 2D hexagonal symmetry between 20 and 200 °C. The pronounced luminescence properties of the mesophase allow one to observe original mesophase textures with flower-like patterns directly by fluorescence microscopy without crossed-polarizers.

## Introduction

Intensive research has focused on the development of functional soft materials through molecular self-assembly. Landmark examples of hierarchical assemblies include micelles, liposomes, microcapsules, dendrimers, colloidal particles, gels, and liquid crystalline materials.[1] Among these soft materials, supramolecular gels and liquid crystalline materials are of particular interest because they can allow to produce one-dimensional stacks of functional molecules and are easily processable without using technologically advanced techniques. On the one hand, discotic liquid crystals possess the ability to self-organize into highly anisotropic and ordered structures such as columns. Molecules forming discotic liquid crystals have, in most cases, a structure that consists of a flat central core with several hydrogenated carbon chains disposed around the outside edge of the core. This specific organization is auspicious for charge separation along the stacks.[2] On the other hand, gel formation by low molecular weight organic gelator (LMWOGs) is induced, in most cases, by the formation of a 3D network of entangled supramolecular fibers. Self-organized one-dimensional assemblies offer great potentials as molecular wires in opto-electronic applications.[3] A particular case demonstrates the potential of thienylvinylene anthracene organogels to provide single-nanofiber transistors.[4]

Along these lines, self-assembly of $\pi$-conjugated molecules into linear structures has attracted much attention because of their potential applications in photonics and optoelectronics, such as field-effect transistors (FETs),[5] organic light emitting diodes (OLEDs),[6] organic light emitting transistors (OLETs),[7] and solar cells.[8] One-dimensional molecular assemblies can be constructed

[†] LCOSA, ECPM.
[‡] IPCMS.
[§] LMSPC, ECPM.
[||] CNR, ISMN.

(1) (a) Hudson, S. D.; Jung, H.-T.; Percec, V.; Cho, W.-D.; Johansson, G.; Ungar, G.; Balagurusamy, V. S. K. *Science* **1997**, *278*, 449. (b) Kukula, H.; Schlaad, H.; Antonietti, M.; Förster, S. *J. Am. Chem. Soc.* **2002**, *124*, 1658. (c) Tedeschi, C.; Li, L.; Möhwald, H.; Spitz, C.; von Seggern, D.; Menzel, R.; Kirstein, S. *J. Am. Chem. Soc.* **2004**, *126*, 3218. (d) Li, L.; Möhwald, H. *Angew. Chem., Int. Ed.* **2004**, *43*, 360. (e) Hoeben, F. J. M.; Jonkheijm, P.; Meijer, E. W.; Schenning, A. P. H. J. *Chem. Rev.* **2005**, *105*, 1491. (f) O'Neill, M.; Kelly, S. M. *Adv. Mater.* **2003**, *15*, 1135. (g) Terech, P.; Weiss, R. G. *Chem. Rev.* **1997**, *97*, 3133. (h) Estroff, L. A.; Hamilton, A. D. *Chem. Rev.* **2004**, *104*, 1201. (i) Tschierske, C. *Chem. Soc. Rev.* **2007**, *36*, 1930.

(2) Schimdt-Mende, L.; Fechtenlötter, A.; Müllen, K.; Moons, E.; Friend, H.; MacKenzie, J. D. *Science* **2001**, *293*, 1119.

(3) (a) Yuen, M.-Y.; Roy, V. A. L.; Lu, W.; Kui, S. C. F.; Tong, G. S. M.; So, M.-H.; Chui, S. S.-Y.; Muccini, M.; Ning, J. Q.; Xu, S. J.; Che, C.-M. *Angew. Chem., Int. Ed.* **2008**, *47*, 9895. (b) Hirst, A. R.; Escuder, B.; Miravet, J. F.; Smith, D. K. *Angew. Chem., Int. Ed.* **2008**, *47*, 8002. (c) Sergeyev, S.; Pisula, W.; Geerts, Y. H. *Chem. Soc. Rev.* **2007**, *36*, 1902. (d) Shimizu, Y.; Oikawa, K.; Nakayama, K.-I.; Guillon, D. *J. Mater. Chem.* **2007**, *17*, 4223. (e) Kumar, S. *Chem. Soc. Rev.* **2006**, *35*, 83.

(4) Hong, J.-P.; Um, M.-C.; Nam, S.-R.; Hong, J.-I.; Lee, S. *Chem. Commun.* **2009**, 310.

  

through weak intermolecular interactions such as hydrogen bonding, $\pi-\pi$ stacking, electrostatic interactions, van der Waals forces, and solvophobic interactions. As a matter of fact, the electronic performances in such electronic devices rely on the intermolecular order in the active layer.

Pyrene is a prototypical molecule, which has high fluorescence quantum yield in solution and shows efficient excimer emission.[9] Pyrene and its derivatives have been extensively applied as biological probes,[10] in photonic devices,[11] and as liquid crystalline materials.[12] Despite its wide use, the fact that the absorption and emission properties of pyrene cores are confined to the UV region constitutes a major drawback. Recently, it has been demonstrated that the absorption and emission characteristics of pyrene can be bathochromatically tuned in the visible region by extending the $\pi$-conjugation upon introduction of ethynyl functions.[13] Pyrene can adequately be functionalized in the 1,3,6,8 positions providing di- or tetrasubstitutions with ethynyl derivatives producing compounds in a controlled manner.[13] Introduction of promesogenic side groups has allowed the synthesis of fluorescent mesomorphic matter, and a stimuli responsive liquid crystalline material in which changes in the photoluminescence emission were triggered by a shear-induced phase transition.[14,15]

In addition, despite their exceptional luminescence properties, ethynyl−pyrene derivatives have not been used up to now to provide robust and highly luminescent low molecular weight gelators. The present contribution fills this gap and uses these organo-gels in field-effect optoelectronic devices. To reach the goal, we used hydrogen-bonding functions such as amide groups to stabilize molecular organizations over larger temperature ranges and to favor the emergence of molecular self-assemblies, for example, organo-gels or liquid crystals.[16] For this purpose, we introduced amide functions between the ethynyl−pyrene core and the promesogenic gallic substituents to stabilize the liquid-crystalline phases over large temperature ranges and to favor the emergence of robust organic gels.

## Results and Discussion

**Synthesis.** The target molecules were prepared by a convergent protocol using 1,6-dibromopyrene[17] or 1,3,6,8-tetrabromopyrene[18] and *N*-(4-ethynylphenyl)-3,4,5-tris(hexadecyloxy)-benzamide with catalytic amounts of palladium(0) (Scheme 1). The latter terminal alkyne was synthesized in two steps from 3,4,5-tris(hexadecyloxy)benzoic acid chloride and 4-trimethylsilylethynylaniline (see the Supporting Information). Compounds **1** and **2** were stable and obtained in good yields and high scales. Their molecular structures and purity were assigned using $^1$H, $^{13}$C NMR, mass spectroscopy, and elemental analysis.

**Spectroscopic Characterizations in Solution and in the Solid State.** The absorption spectra of compound **1** in diluted dichloromethane solutions show two main absorption band peaks at 431 and 411 nm (Table 1). The absorption bands located at higher energies (307, 295, and 250 nm) are likely due to $\pi-\pi^*$ and $n-\pi^*$ transitions localized on the alkoxyphenyl fragments (Figure 1a). The absorption spectrum of compound **2** is similar but shows a pronounced bathochromic shift of the main absorption band peaks now located at 482 and 458 nm (Figure 1b). Exciting the low energy absorption bands of compound **1** leads to strong emissions at 445 nm (0−0 transition) and 473 nm (0−1 transition) with a quantum yield of 95% (Table 1 and Figure 1a). The fluorescence spectrum shows relatively good mirror symmetry with respect to the lowest energy absorption transitions, confirming that the same optical transitions are involved in both absorption and emission processes. The small Stokes shift observed is due to substantial invariance of the molecular geometric structure in the ground ($S_0$) and the first excited ($S_1$) states, while the perfect match between the excitation and absorption spectra points to the efficient radiative deactivation of the excited electronic state. The fluorescence


(5) (a) van de Craats, A. M.; Stutzmann, N.; Bunk, O.; Nielsen, N. N.; Watson, M.; Müllen, K.; Chanzy, H. D.; Sirringhaus, H.; Friend, R. H. *Adv. Mater.* **2003**, *15*, 495. (b) Pisula, W.; Menon, A.; Stepputat, M.; Lieberwirth, I.; kolb, U.; Tracz, A.; Sirringhaus, H.; Pakula, T.; Müllen, K. *Adv. Mater.* **2005**, *17*, 684. (c) Kitamura, T.; Nakaso, S.; Mizoshita, N.; Tochigi, Y.; Shimomura, T.; Moriyama, M.; Ito, K.; Kato, T. *J. Am. Chem. Soc.* **2005**, *127*, 14769.

(6) (a) Mitschke, U.; Bäuerle, P. *J. Mater. Chem.* **2000**, *10*, 1471. (b) Hassheider, T.; Benning, S. A.; Kitzerow, H.-S.; Achard, M.-F.; Bock, H. *Angew. Chem., Int. Ed.* **2001**, *40*, 2060.

(7) (a) Muccini, M. *Nature Materials,* **2006**, *5*, 605. (b) Loi, M. A.; Da Como, E.; Dinelli, F.; Murgia, M.; Zamboni, R.; Biscarini, F.; Muccini, M. *Nat. Mater.* **2005**, *4*, 81.

(8) (a) Greeg, B. A.; Fox, M. A.; Bard, A. J. *J. Phys. Chem.* **1990**, *94*, 1586. (b) Fox, A. M.; Grant, J. V.; Melamed, D.; Torimoto, T.; Liu, C.-Y.; Bard, A. J. *Chem. Mater.* **1998**, *10*, 1771. (c) Kubo, W.; Kambe, S.; Nakade, S.; Kitamura, T.; Hanabusa, K.; Wada, Y.; Yanagida, S. *J. Phys. Chem. B* **2003**, *107*, 4374.

(9) Förster, T.; Kasper, K. *Z. Electrochem.* **1955**, *59*, 976.

(10) (a) Okamoto, A.; Kanatani, K.; Saito, I. *J. Am. Chem. Soc.* **2004**, *126*, 4820. (b) Fujimoto, K.; Shimizu, H.; Inouye, M. *J. Org. Chem.* **2004**, *69*, 3271. (c) Han, M. K.; Lin, P.; Paek, D.; Harvey, J. J.; Fuior, E.; Knutson, J. R. *Biochemistry* **2002**, *41*, 3468–3476. (d) Langenegger, S. M.; Häner, R. *Chem. Commun.* **2004**, 2792.

(11) (a) Otsubo, T.; Aso, Y.; Takamiya, K. *J. Mater. Chem.* **2002**, *12*, 2565. (b) Jia, W.-L.; McCormick, T.; Liu, Q.-D.; Fukutani, H.; Motala, M.; Wang, R.-Y.; Tao, Y.; Wang, S. *J. Mater. Chem.* **2004**, *14*, 3344. (c) Tang, C.; Liu, F.; Xia, Y.-J.; Lin, J.; Xie, L.-H.; Zhong, G.-Y.; Fan, Q.-L.; Huang, W. *Org. Electron.* **2006**, *7*, 155–162. (d) Oh, H.-Y.; Lee, C.; Lee, S. *Org. Electron.* **2009**, *10*, 13.

(12) (a) Benning, S. A.; Hassheider, T.; Keuker-Baumann, S.; Bock, H.; Della Sala, F.; Frauenheim, T.; Kitzerow, H.-S. *Liq. Cryst.* **2001**, *28*, 1105. (b) Percec, V.; Glodde, M.; Bera, T. K.; Miura, Y.; Shiyanovskaya, I.; Singer, K. D.; Balagurusamy, V. S. K.; Heiney, P. A.; Schnell, I.; Rapp, A.; Spiess, H.-W.; Hudson, S. D.; Duan, H. *Nature* **2002**, *419*, 384. (c) de Halleux, V.; Calbert, J. P.; Brocorens, P.; Cornil, J.; Declercq, J. P.; Brédas, J. L.; Geerts, Y. *Adv. Funct. Mater.* **2004**, *14*, 649. (d) Kamikawa, Y.; Kato, T. *Org. Lett.* **2006**, *8*, 2463. (e) Kim, Y. H.; Yoon, D. K.; Lee, E. H.; Koan, Y. K.; Jung, H.-T. *J. Phys. Chem. B* **2006**, *110*, 20836. (f) Sienkowska, M. J.; Monobe, H.; Kaszynski, P.; Shimizu, Y. *J. Mater. Chem.* **2007**, *17*, 1392. (g) Sienkowska, M. J.; Farrar, J. M.; Zhang, F.; Kusuma, S.; Heiney, P. A.; Kaszynski, P. *J. Mater. Chem.* **2007**, *17*, 1399.

(13) (a) Maeda, H.; Maeda, T.; Mizuno, K.; Fujimoto, K. *Chem.-Eur. J.* **2006**, *12*, 824. (b) Venkataramana, G.; Sankararaman, S. *Org. Lett.* **2006**, *8*, 2739. (c) Venkataramana, G.; Sankararaman, S. *Eur. J. Org. Chem.* **2005**, 4162. (d) Zhao, Z.; Li, J.-H.; Chen, X.; Lu, P.; Yang, Y. *Org. Lett.* **2008**, *10*, 3041. (e) Kim, H. M.; Lee, Y. O.; Lim, C. S.; Kim, J. S.; Cho, B. R. *J. Org. Chem.* **2008**, *73*, 5127. (f) Leroy-Lhez, S.; Fages, F. *Eur. J. Org. Chem.* **2005**, 2684. (g) Xing, Y.; Xu, X.; Zhang, P.; Tian, W.; Yu, G.; Lu, P.; Liu, Y.; Zhu, D. *Chem. Phys. Lett.* **2005**, *408*, 169. (h) Zhao, Z.; Xu, X.; Jiang, Z.; Lu, P.; Yu, G.; Liu, Y. *J. Org. Chem.* **2007**, *72*, 8345. (i) Xiao, J.; Li, J.; Li, C.; Huang, C.; Li, Y.; Cui, S.; Wang, S.; Liu, H. *Tetrahedron Lett.* **2008**, *49*, 2656. (j) Shimizu, H.; Fujimoto, K.; Furusyo, M.; Maeda, H.; Nanai, Y.; Mizuno, K.; Inouye, M. *J. Org. Chem.* **2007**, *72*, 1530. (k) Xiao, J.; Xu, J.; Cui, S.; Liu, H.; Wang, S.; Li, Y. *Org. Lett.* **2008**, *10*, 645. (l) Bernhardt, S.; Kastler, M.; Enkelmann, V.; Baumgarten, M.; Müllen, K. *Chem.-Eur. J.* **2006**, *12*, 6117.

(14) (a) Sagara, Y.; Kato, T. *Angew. Chem., Int. Ed.* **2008**, *47*, 5175. (b) Kamikawa, Y.; Kato, T. *Langmuir* **2007**, *23*, 274.

(15) Hayer, A.; de Halleux, V.; Kölher, A.; El-Garoughy, A.; Meijer, E. W.; Barbera, J.; Tant, J.; Lein, J.; Lehmann, M.; Gierschner, J.; Cornil, J.; Geerts, Y. H. *J. Am. Chem. Soc.* **2006**, *110*, 7653.

(16) Ziessel, R.; Camerel, F.; Donnio, B. *Chem. Rec.* **2009**, *9*, 1.

(17) Grimshaw, J.; Grimshaw, J. T. *J. Chem. Soc., Perkin Trans. 1* **1972**, 1622.

(18) Kim, H. M.; Lee, Y. O.; Lim, C. S.; Kim, J. S.; Cho, B. R. *J. Org. Chem.* **2008**, *73*, 5127.

**Scheme 1** [a]

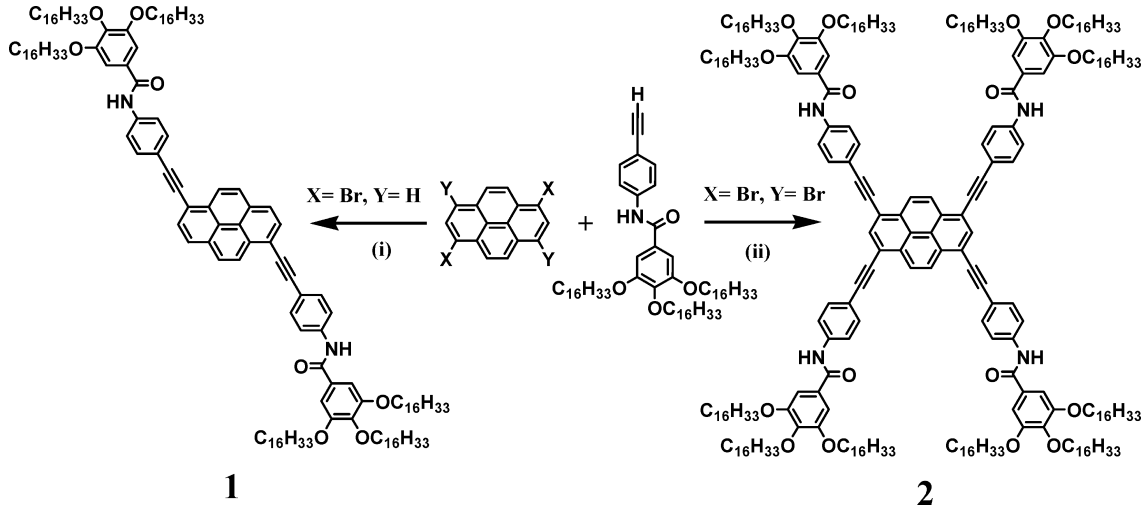


[a] Reagents and conditions: (i) 1,6-dibromopyrene, *N*-(4-ethynylphenyl)-3,4,5-tris(hexadecyloxy)benzamide (2.2 equiv), *n*-propylamine, [$Pd(PPh_3)_4$], 60 °C, overnight, 74%; (ii) 1,3,6,8-tetrabromopyrene, *N*-(4-ethynylphenyl)-3,4,5-tris(hexadecyloxy)benzamide (6 equiv), piperidine, [$Pd(PPh_3)_4$], 90 °C, 20 h, 54%.

***Table 1.*** Optical Data Measured in Dichloromethane Solution at 298 K

| | $\lambda_{abs}$ (nm) | $\varepsilon$ ($M^{-1}$ $cm^{-1}$) | $\lambda_F$ (nm) | $\Phi_F$[a] | $\tau_F$ (ns) | $k_r$[b] ($10^8$ $s^{-1}$) | $k_{nr}$[b] ($10^8$ $s^{-1}$) |
|---|---|---|---|---|---|---|---|
| **1** | 431 | 59 500 | 445 | 0.95 | 1.1 | 8.64 | 0.45 |
| | 411 | 62 500 | 473 | | | | |
| | 307 | 60 800 | | | | | |
| | 295 | 54 300 | | | | | |
| | 250 | 38 700 | | | | | |
| **2** | 482 | 51 000 | 504 | 0.85 | 2.1 | 4.04 | 0.71 |
| | 458 | 48 200 | 539 | | | | |
| | 362 | 93 400 | | | | | |
| | 293 | 69 000 | | | | | |

[a] Determined in dichloromethane solution ($c \approx 1.10^{-6}$ M) using Rhodamine 6G as reference ($\Phi_F = 0.78$ in water, $\lambda_{exc} = 488$ nm).[19] All $\Phi_F$ values are corrected for changes in refractive index. [b] Calculated using the following equations: $k_r = \Phi_F/\tau_F$, $k_{nr} = (1 - \Phi_F)/\tau_F$, assuming that the emitting state is produced with unit quantum efficiency.

decay profiles can be well-fitted by a single exponential curve, with a fluorescence lifetime of 1.1 ns.

Excitation of compound **2** in the lowest energy bands also leads to an intense emission centered at 504 and 539 nm with a quantum yield of 85% (Figure 1b). The symmetry of emission band, the fluorescence decay profile (which can be well-fitted by a single exponential curve with fluorescence lifetime of 2.1 ns), together with the small Stokes shift observed are in accordance with an individual singlet excited state. The emission is red-shifted by ∼60 nm, as compared to compound **1** (Table 1). This bathochromic shift suggests an efficient delocalization in the excited state. Introduction of two ethynyl fragments on the pyrene unit leads to a bathochromic shift of ∼20 nm as compared to a naked pyrene ($\lambda_{em} = 420$ nm),[9] and introduction of four ethynyl fragments leads to a bathochromic shift of almost 100 nm. Extension of the molecular size with the introduction of conjugated ethynyl−phenyl fragments can efficiently tune the luminescence properties from the UV to the visible region.

Emission properties of compounds **1** and **2** in the solid state were also evaluated directly on the powders thanks to a spectrofluorimeter equipped with an optical fiber Figure 1 (dotted lines). Fluorescence spectra are red-shifted with maxima at 502 and 670 nm for **1** and **2**, respectively, as compared to the emission maxima measured in diluted solutions. For **2**, the large red-shift together with the broad and featureless emission profile is likely due to the formation of excimers in the solid state.[9,15] In the solid state, the more red-shifted PL emission spectra of compound **2** (166 nm at peak maximum) with respect to compounds **1** (57 nm at peak maximum) likely suggest that the molecular arrangement of the bisubstituted compound **1** leads to weaker intermolecular interactions that prevent the formation of excimers. Indeed, the more resolved PL spectrum of compound **1** in the solid state corroborates this hypothesis.

**Gelation Properties.** Gelation of organic solvents by low molecular weight gelators is typified by the formation of a stable three-dimensional, noncovalent network structure through intricate intermolecular interactions, such as hydrogen bonding, $\pi-\pi$ stacking, and hydrophobic effect with the solvent. The presence of a large aromatic core and amide functions on the ambipolar compounds **1** and **2** led us to probe their gelation abilities in various polar or nonpolar, protic or nonprotic solvents (see Table S1). For gelation tests, 5 mg of compound was mixed with 0.2 mL of solvent in a septum-capped vial. The mixture was heated until the solid was completely dissolved. The resulting clear solution was cooled in air to room temperature and left overnight to complete the gelation. The gel formation criteria used was to verify the absence of flowing of the solution when the test tube was turned upside-down at room temperature. Compound **2** was found to be deprived of gelation ability, and precipitation always occurs in the tested solvent upon cooling after solubilization at elevated temperatures. The presence of four donor−acceptor functions in **2** invariably leads to greater intermolecular interactions and to better aggregation capabilities leading to a higher tendency toward precipitation. On the contrary, a subtle balance between precipitation and solubilization was found with compound **1**. The bisamide pyrene compound was found to be able to gel solvents such as cyclohexane, toluene, and dimethylformamide. Transparent gels were formed in cyclohexane, and turbid gels were formed in toluene and DMF at 25 °C. In each case, the complete volume of solvent is immobilized and can support its own weight without collapsing as shown in Figure 2. The organogels exhibited thermally reversible sol to gel phase transitions. When

(19) Olmsted, J. *J. Phys. Chem.* **1979**, *83*, 2581.

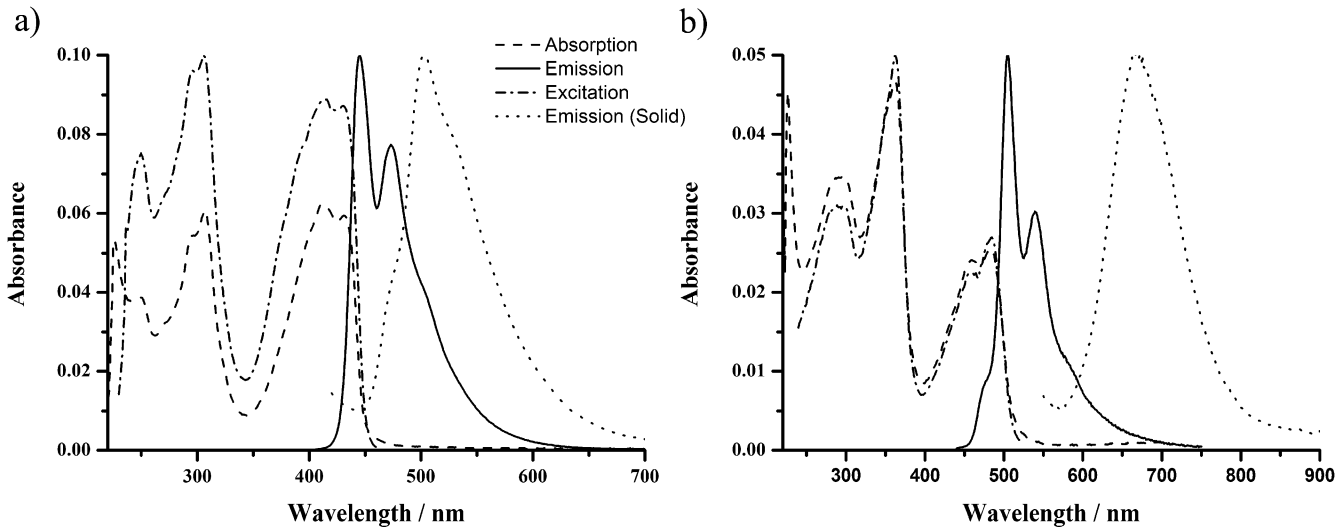


***Figure 1.*** (a) For **1**, absorption, emission ($\lambda_{ex} = 390$ nm), and excitation ($\lambda_{em} = 473$ nm) spectra in dichloromethane ($c = 1.0 \times 10^{-6}$ mol $L^{-1}$) and emission spectrum of the solid at room temperature ($\lambda_{ex} = 420$ nm). (b) For **2**, absorption, emission ($\lambda_{ex} = 430$ nm), and excitation ($\lambda_{em} = 538$ nm) spectra in dichloromethane ($c = 0.5 \times 10^{-6}$ mol $L^{-1}$) and emission spectrum of the solid at room temperature ($\lambda_{ex} = 450$ nm).

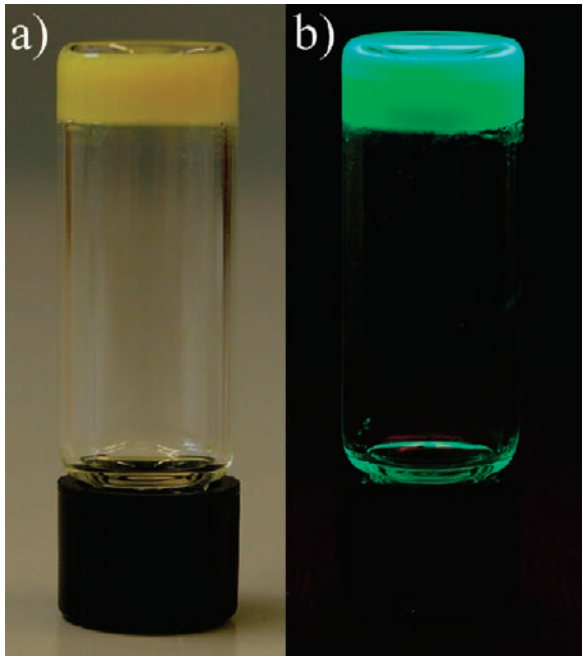


***Figure 2.*** (a) Gelation test of the compound **1** in DMF (5 mg/0.2 mL). (b) Same gel observed upon UV irradiation at 365 nm.

observed upon UV irradiation, these gels appear strongly luminescent (Figure 2b).

Spectroscopic measurements show that the emission properties of the gel depend on the nature of the solvent used. In DMF, the gels display a strong structured emission band centered at 500 nm (Figure 3). The 0−1 vibronic peak (500 nm) appears more intense than the 0−0 vibronic peak (475 nm). The position of the emission band, which is slightly red-shifted by 27 nm as compared to the emission band in diluted solutions of compound **1**, together with a well-resolved emission profile indicates the relatively weak interactions among molecules. In toluene gels, a well-structured emission centered at 497 nm is also observed. Moreover, in this solvent, the 0−0 vibronic peak is more intense than in DMF, and the 0−2 is clearly observed at 479 nm. Interestingly, in cyclohexane gels, the emission band that is still centered at 501 nm is less structured, broader, and more

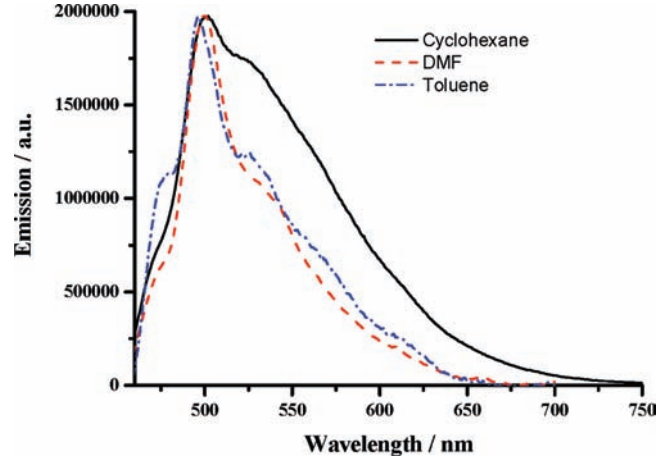


***Figure 3.*** Emission spectra of compound **1** in cyclohexane, toluene, and DMF gels ($c = 25$ g $L^{-1}$) ($\lambda_{ex} = 450$ nm).

extended toward the higher wavelengths. The shape and the full-width-at-half-maximum (fwhm) of the emission band indicate that in cyclohexane favorable $\pi-\pi$ interactions between the pyrene core and the solvent can induce higher electronic stabilization in the fiber formation process.

The morphology of the gel structure was examined by scanning electron microscopy (SEM). Figure 4 shows the electron micrographs of xerogels deposited on silicon wafer from compound **1** in cyclohexane, toluene, and DMF. The micromorphology of the gels is strongly dependent on the nature of the gelating solvent. In cyclohexane, the xerogel appeared as a 3D network of interlocked thin fibers with diameter in the range 40−70 nm extending over micrometers (Figure 4a). The mean diameter observed for the fibers (∼55 nm) is larger than the one expected for a single molecular chain, thereby suggesting that the xerogels are constituted of superbundles resulting from the intertwining of several molecular chains. In toluene, a similar 3D network of fibers extending over several tens of micrometers can be observed, but the diameter of the formed one-dimensional assemblies is larger and is in the range 50−110 nm with a mean diameter of 70 nm (Figure 4b). The larger size of the fibers observed in the toluene gels accounts for the highest robustness

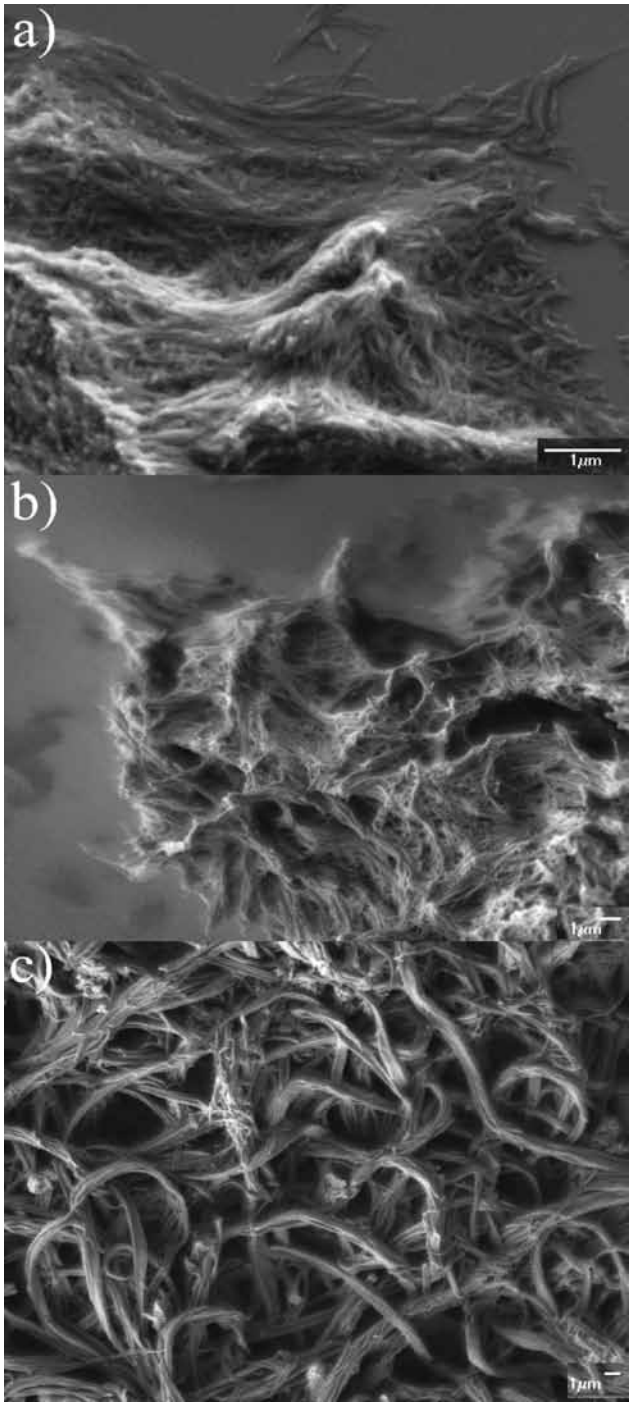


***Figure 4.*** SEM images of xerogels of compound **1** in (a) cyclohexane, (b) toluene, and (c) dimethylformamide deposited on silicon wafer ($c$ = 25 g $L^{-1}$).

of the toluene gels as compared to cyclohexane gels. In DMF, the morphology of the gel freeze-dried on silicon wafer appeared completely different. Gel formation in DMF arises from the formation of a dense network of entangled fibers with diameter in the range 500−1000 nm, which is 1 order of magnitude higher than the two previous gels in cyclohexane and in toluene (Figure 4c). A closer look reveals that these large fibers in DMF are formed by smaller elementary fibers (∅ = 100−150 nm) (Figure S1). The large fibers look like ropes and are formed by the aggregation/intertwining of smaller size elementary fibers. The mean diameter of the elementary fibers is large as compared to the molecular dimensions, and they are themselves formed by the intertwining of several molecular chains (10−50 elementary fibers per rope).

The role of hydrogen bonding in the formation of the observed fibers was ascertained by infrared spectroscopy in cyclohexane, toluene, and DMF gels (25 g $L^{-1}$). A single C═O stretching band was observed at 1644, 1643, and 1659 $cm^{-1}$, in cyclohexane, toluene, and DMF, respectively. Furthermore, a large NH stretching vibration at 3261 $cm^{-1}$ in cyclohexane, 3265 $cm^{-1}$ in toluene, and 3332 $cm^{-1}$ in DMF was observed in the gelled solvents. These spectroscopic data are an unambiguous signature of hydrogen-bonded amides inducing a hydrogen-bonded network, in line with the aggregation of the ligands into elongated fibers (vide supra). It can also be supposed that the presence of $\pi-\pi$ interactions among pyrene cores, highlighted by the fluorescence measurements, and/or among phenyl subunits might add additional stabilization interactions. Gel formation in DMF can be viewed as a three-step hierarchical supramolecular assembly. First, the molecules are assembled, through hydrogen bonding, $\pi-\pi$ interactions, and van der Waals interactions of the paraffin chains, into one-dimensional extended assemblies, and then these molecular chains intertwine together to form the elementary fibers with a mean diameter around 120 nm. Ultimately these elementary fibers further intertwine to form large ropes of larger diameters. The formation of these large rope-like assemblies in the DMF gels accounts for their higher robustness and opacity.

**Laser Scanning Confocal Microscopy of the Gel of Compound 1.** Laser scanning confocal microscope (LSCM) images obtained from partially dissolved xerogel in DMF drop-cast on a microscope coverslip are presented in Figure 5. The images reveal a dense 3D network of greenish fluorescent cylindrical strands, which is fairly related to the SEM images. The fiber entanglement presents an irregular distribution of diameters and lengths. Even though the in-plane resolution of the LSCM (∼200 nm) is lower than that of the SEM, we can distinguish at a smaller field of view (Figure 5b) that the fibrous structure turned out to be bundles of intertwining fibers with smaller mean diameters.

To gain information on the photophysical properties of the pyrene-derivative fibers at the nano scale, localized PL spectroscopy was performed in the regions that are delimited by 2.5 × 2.5 $\mu m^2$-wide squares in Figure 5a and b. In particular, we aim at studying a large fiber bundle in an assembly of entangled fibers (Figure 5a) and an isolated bundle of intertwined fibers (Figure 5b).

In both cases, the spectra profile and peak positions are nearly invariant regardless of the spatial position of the PL measurements (Figure 6). In particular, a well-defined vibronic progression is present with almost five detectable peaks. With respect to the solution PL spectrum (Figure 1a), the vibronic progression is dominated by the 0−1 transition, the emission broadens, and the vibronic energy difference maintains invariant (∼0.17 eV). Moreover, the 0−1 vibronic peak wavelength does not change, but the vibronic progression (especially the 0−2 peak) is much more resolved as compared to the diluted solution.

Differently from other pyrene-derivative molecules in the aggregate state,[20,21] the emission of compound **1** arranged in fibers cannot be simulated successfully by the superimposition

(20) Winnik, F. M. *Chem. Rev.* **1993**, *93*, 587.
(21) Da Como, E.; Loi, M. A.; Murgia, M.; Zamboni, R.; Muccini, M. *J. Am. Chem. Soc.* **2006**, *128*, 4277.

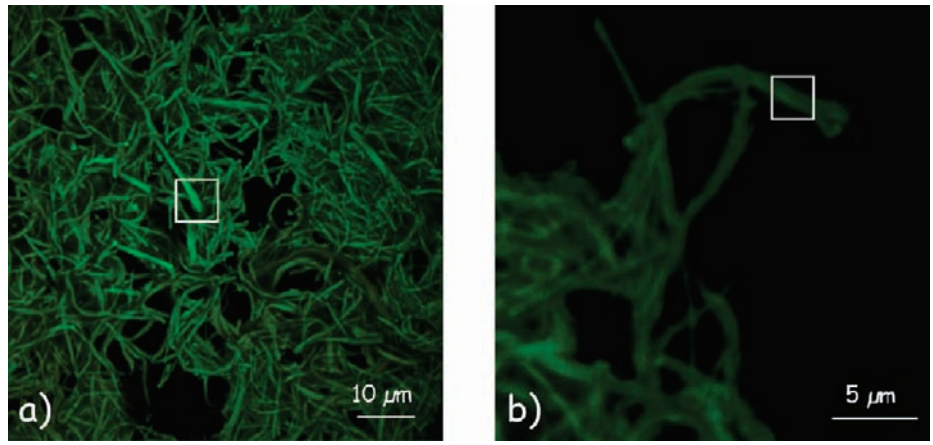


***Figure 5.*** 80 × 80 $\mu m^2$ (a) and 25 × 25 $\mu m^2$ (b) LCSM images of xerogels of compound **1** in DMF deposited on a microscope coverslip. Excitation wavelength 408 nm and 60× oil-immersion microscope objective.

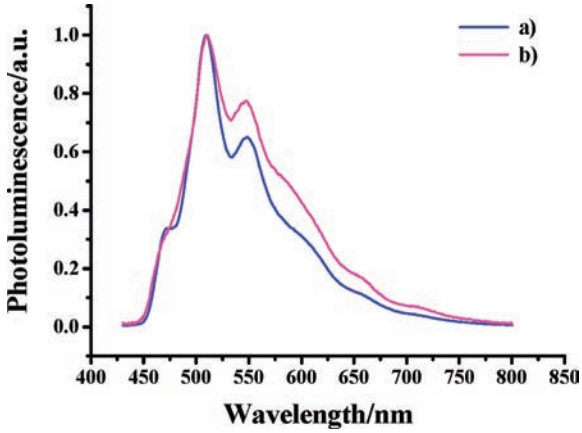


***Figure 6.*** Localized PL spectra of the xerogel of compound **1** in DMF deposited on a microscope coverslip. The spectra labeled as (a) and (b) are collected from the 2.5 × 2.5 $\mu m^2$-wide regions in images reported in Figure 5a and b, respectively.

of a monomer band with a vibronic progression similar to the one of the solution PL spectrum together with broad, structureless, and red-shifted excimer bands. Because the progression is dominated by the 0−1 line with a slight fwhm reduction with respect to the solution,[22,23] we hypothesize that pyrene moieties tend to form H-type aggregates with $\pi-\pi$ stack along the fiber axis. In particular, it is likely that the presence of hydrogen bonding among the molecular units allows the fiber to arrange in a suitable 3D architecture that prevents efficient excimer formation. Indeed, it is well-known that excimer formation depends upon the distance between the facing molecules.[24] Considering the PL spectrum of a fiber bundle in an assembly of entangled fibers (Figure 6, curve a), the well-resolved vibronic progression shows that the alkyl spacer gelificators localized at the rim of the fiber columnar structure inhibit the interaction among fibers.

Nonetheless, we cannot conclude that the inhomogeneous broadening of the wide-field PL spectrum of the xerogel in DMF (Figure 3) is due only to interbundle structural disorder because the PL localized spectrum of the isolated bundle (Figure 6, curve b) shows a redistribution of the oscillator strengths within the vibronic progression and a broadened emission.

So the spectroscopic fingerprints of localized PL spectra correlated to the morphological features of the LSCM images highlight the role of the single fiber bundle structural order and that of the interactions among different bundles.

**Electronic Properties in OFET Devices of the Gel Formed with Compound 1.** To evaluate the electronic properties of the pyrene-derivative xerogel in a technologically appealing electronic device structure, top-contact/bottom gate organic field-effect transistors (OFETs)[25] with compound **1** as active layer were fabricated using a spin-coated film of the fibers obtained from DMF gels (see experimental section in the Supporting Information).

The collected locus electrical characteristics highlight that a good bulky transport for both electrons and holes takes place from source to drain electrodes (Figure 7). Indeed, the output characteristics (not reported here) reveal an almost negligible modulation of the drain-source current due to the application of a gate voltage.

From the structural and morphological investigations, a continuum of micrometer-long fibers can likely connect source and drain electrodes, allowing charge transport across fiber bundles without the formation of a charge accumulation layer. Moreover, it was observed that increasing the quantity of material forming the active layer led to an increase of the current flowing from source to drain electrodes as it is expected because the spin-coated film is much more uniform and a higher amount of percolating paths are present.

The light emission collected in the high source-drain voltage region can be attributed to a well-known diode-like process[26] of exciton formation and radiative recombination in the proximity of the metal electrodes, which is typically present in field-effect devices based on luminescent active materials.

The lack of field effect in the top-contact OFET devices could be favored by the inhomogeneous coverage of the metallic

(22) Oelkrug, D.; Egelhaaf, H.-J.; Gierschner, J.; Tompert, A. *Synth. Met.* **1996**, *76*, 249.
(23) Muccini, M.; Lunedei, E.; Bree, A.; Horowitz, G.; Garnier, F.; Taliani, C. *J. Chem. Phys.* **1998**, *108*, 7327.
(24) Jun, E. J.; Won, H. N.; Kim, J. S.; Leec, K.-H.; Yoon, J. *Tetrahedron Lett.* **2006**, *47*, 4577.
(25) (a) Cicoria, F.; Santato, C.; Dinelli, F.; Murgia, M.; Loi, M. A.; Biscarini, F.; Zamboni, R.; Heremans, P.; Muccini, M. *Adv. Funct. Mater.* **2005**, *15*, 375. (b) Gomes, H. L.; Stallinga, P.; Dinelli, F.; Murgia, M.; Biscarini, F.; De Leeuw, D. M.; Muccini, M.; Müllen, K. *Polym. Adv. Technol.* **2005**, *16*, 227. (c) Xu, Z.-X.; Roy, V. A. L.; Stallinga, P.; Muccini, M.; Xiang, H.-F.; Che, C.-M. *Appl. Phys. Lett.* **2007**, *90*, 223509.

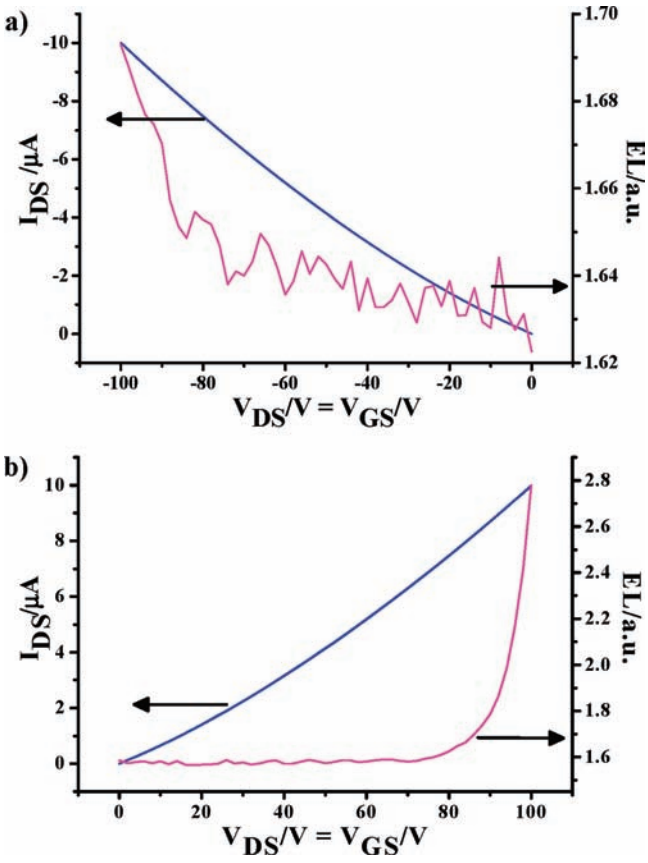


***Figure 7.*** Locus characteristics and corresponding electroluminescence (EL) of a top-contact and bottom-gate FET in p polarization (a) and n polarization (b) having pyrene-derivative fibers from compound **1** as the active layer.

contacts on the organic film. Therefore, to prevent this issue and check the field-effect response, bottom-contact/bottom-gate OFETs with n-doped silicon substrate as a gate electrode, a 300 nm thick silicon dioxide layer as a gate dielectric, prepatterned gold source and drain electrodes, and a spin-coated active layer were realized. Also, in this case, no modulation of the source-drain current from the applied gate voltage was detected.

We note that, given the bulk electrical conductivity, the optical emission properties, as well as the morphological arrangement of fibers in the xerogel, this material could likely be used for the realization of fiber-based organic light-emitting diodes. However, we do not exclude a priori that compound **1** may be implemented in the realization of field-effect devices by means of a proper treatment of the dielectric surface aimed at inducing a suitable packing of the molecular units, which in principle can enhance the charge accumulation and the field-effect charge flow.[4]

**Mesomorphic Behavior.** Thermal behavior of the compounds **1** and **2** was investigated by polarizing optical microscopy (POM) and differential scanning calorimetry (DSC), and the transition temperatures and enthalpies are gathered in Table S2 and Figure S2. The hexacatenar compound **1** is not mesomorphic and melts directly into the isotropic liquid above 177 °C.

DSC traces of the cross-like compound **2** display two reversible thermal transitions centered at 27 and 218 °C on the heating curves and at 205 and 19 °C on the cooling curves (Figure S3). Above 218 °C, **2** is a isotropic fluid, and the material appears completely dark under crossed polarizers. On cooling, the material becomes birefringent below 205 °C, and a texture readily develops under crossed-polarizers. The observed texture, which is characterized by dark, homeotropically aligned regions and birefringent filaments (chromosome-like motifs), indicates the formation of an optically uniaxial columnar phase (Figure 10a and Figure S4). Shearing converts the structured texture into an unspecific, homogeneous birefringent texture, which indicates the fluid-like nature of the material. Below 19 °C, no clear textural change is observed, and the texture is hardly damaged by shearing. The high enthalpy value measured on the DSC curves associated with this transition indicates the formation of a crystalline phase below 19 °C.

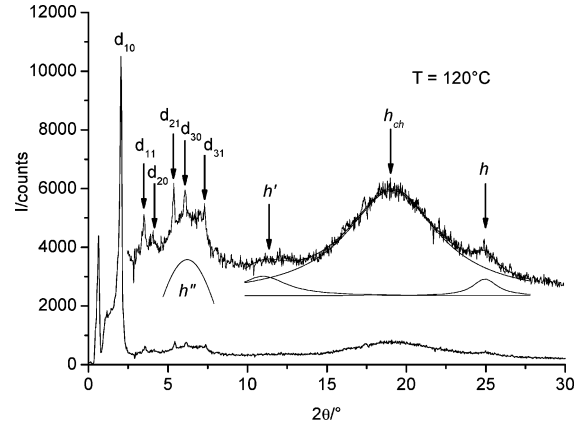


***Figure 8.*** Diffraction pattern of compound **2** at $T = 120$ °C.

Small-angle X-ray diffraction for compound **2** confirmed the POM observations and DSC experiments. At low temperatures, the X-ray patterns exhibit Bragg reflections, which sharpen and become more intense on continuing heating (above 80 °C), until the isotropization temperature is reached, where all of the sharp reflections collapsed. The XRD pattern recorded at 120 °C, taken as a representative example, is shown in Figure 8. It is characterized by the presence of seven sharp small-angle X-ray reflections, with reciprocal spacings in the ratio $1:\sqrt{3}:2:\sqrt{7}:3:\sqrt{12}:\sqrt{13}$. These features are most readily assigned as the (10), (11), (20), (21), (30), (22), and (31) reflections of a hexagonal lattice with a parameter $a = 51.7$ Å (Table S3). In addition to these fine reflections, four other, but diffuse, scatterings were also observed. The most intense one, denoted as $h_{ch}$, is connected to the molten aliphatic chains, in liquid-like conformation. The other three diffuse scatterings were measured as $h$ (3.6 Å), $h'$ (7.2 Å), and $h''$ (14.2 Å, $h''$ overlapping with the small angle reflections), corresponding, respectively, to intermolecular $\pi-\pi$ stacking and modulation along the main axis ($h' = 2h$, $h'' = 4h$). The same X-ray patterns were obtained for the other temperatures, confirming the presence of one single $Col_h$ phase throughout the temperature range. In addition, the lattice parameter of the mesophase is quasi constant with temperature ($a = 50-52$ Å), implying little molecular rearrangement within the columns, and that the variation of the molecular volume in this temperature range is solely governed by that of the aliphatic chains. The column formation results from the one-dimensional stacking of these nearly disk-like molecules on top of each other (one molecule per 3.0 Å, see supporting information) with a continuous alternation of the molecular plane tilt, generating a pseudohelix. This conformation is further facilitated owing to the cross-like molecular shape, which permits the lateral arms

(26) (a) Santato, C.; Capelli, R.; Loi, M. A.; Murgia, M.; Cicoria, F.; Roy, V. A. L.; Stallinga, P.; Zamboni, R.; Rost, C.; Karg, S. F.; Muccini, M. *Synth. Met.* **2004**, *146*, 329. (b) Rost, C.; Karg, S.; Riess, W.; Loi, M. A.; Murgia, M.; Muccini, M. *Synth. Met.* **2004**, *146*, 237.

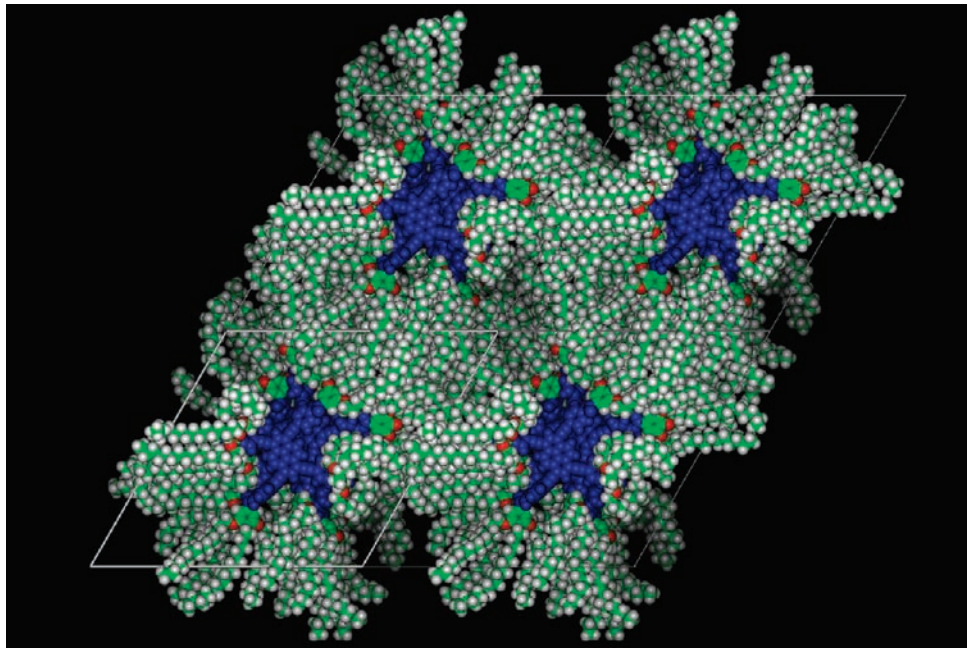

***Figure 9.*** View of the molecular packing obtained after dynamic simulation of the columnar tilted arrangement.

to occupy the available space then generated (interdigitation), and to interact through hydrogen bond interactions. Molecular dynamic simulation confirms that 4 molecules of pyrene stacked one on top of the other in a helicoidal fashion (see the Supporting Information and Figures S5 and S6) with a periodicity of 12.2 Å. Such a helical stacking of the molecules in the column could account for the modulations observed in the X-ray pattern, and $h'$ and $h''$ could therefore be related to the existence of a superlattice periodicity in the direction of the stacks of molecules (Figure 9). Of course, such a helicoidal stacking is short-range and not correlated between the columns.

**Textural Characterizations of the $Col_h$ Phase of Compound 2 by Luminescence Microscopy.** Recently, it has been demonstrated that luminescence properties of liquid crystalline phases can be exploited to probe the molecular organization in thin films at the macroscopic scale by fluorescence microscopy.[27,28] For these reasons, the emission properties of compound **2** in the various material states detected by DSC and XRD were evaluated with the help of a fluorescence microscope equipped with a heating stage.

Compound **2** appears highly luminescent in the solid state upon UV irradiation in the range 300−350 nm (Figure S7). The observed red luminescence confirms the measurements performed by fluorescence spectroscopy on solid powder and testifies the formation of aggregated species in the solid material. The emission spectrum recorded on the solid powder at room temperature displays a broad and unstructured emission band centered at 675 nm (Figure 1b). At temperatures above 218 °C, the material is in the isotropic state, and all of the molecules are randomly distributed. The luminescence appears orange and completely uniform inside the fluid material (Figure S8). Observation of blue-shifted emission points to a disaggregation process induced by the increase of the thermal motion at elevated temperatures. It is interesting to note that the luminescence remains pronounced even at high temperatures. The observed orange emission ($\lambda = 625$ nm), which is red-shifted as compared to the emission of the isolated species in dichloromethane solution ($\lambda = 504$ and 539 nm), also indicates that local stacking of the pyrene cores persists in the isotropic phase. Upon cooling below 205 °C, the material enters in the liquid-crystalline state, and the typical texture of the hexagonal columnar phase, with birefringent chromosome-like domains and large homeotropic regions (dark regions), is observed by classical POM (Figure 10a). The red luminescence observed ($\lambda_{em} = 675$ nm) upon irradiation at $300 < \lambda_{ex} < 350$ nm without any polarizer is not uniform anymore, and domains with different emission can be observed (Figure 10b). The emission of the different bright and dark domains likely matches the texture observed in transmission between crossed-polarizers (Figure 10c). Interestingly, the chromosome-like motifs detected by POM are almost nonluminescent, whereas, in place of the homeotropic domains, flower-like highly luminescent motifs appear. The number of petals of the flowers is always six, which perfectly reflects the 6-fold symmetry of the mesophase ($Col_h$). In the homeotropic domains, the columns are oriented perpendicular to the glass surface, and they are arranged in a two-dimensional lattice of hexagonal symmetry. The observation of luminescent six petals flower-like motifs is a direct visualization of the symmetry of the 2D organization of the columns. The sizes of the flower-like motifs are in the range 2−8 $\mu$m, which is very large as compared to the surface of a column. The flower-like domains correspond approximatively to a two-dimensional assembly of $1 \times 10^5$ to $2 \times 10^6$ columns. Some flowers present a black circular nonemissive area in the center, whereas some others have a completely uniform luminescence. The origin of this black circular area is not completely clear, but it can arise from destructive emissive interferences or from a peculiar orientation of the columnar axis with respect to the normal of the surface or with respect to the direction of the excitation beam. The luminescence texture observed reveals that the columns oriented

(27) (a) Camerel, F.; Bonardi, L.; Retailleau, P.; Ziessel, R. *J. Am. Chem. Soc.* **2006**, *128*, 4548. (b) Camerel, F.; Bonardi, L.; Ulrich, G.; Charbonnière, L.; Donnio, B.; Bourgogne, C.; Guillon, D.; Retailleau, P.; Ziessel, R. *Chem. Mater.* **2006**, *18*, 5009. (c) Camerel, F.; Ulrich, G.; Barbera, J.; Ziessel, R. *Chem.-Eur. J.* **2007**, *13*, 2189.
(28) Binnemans, K. *J. Mater. Chem.* **2009**, *19*, 448.

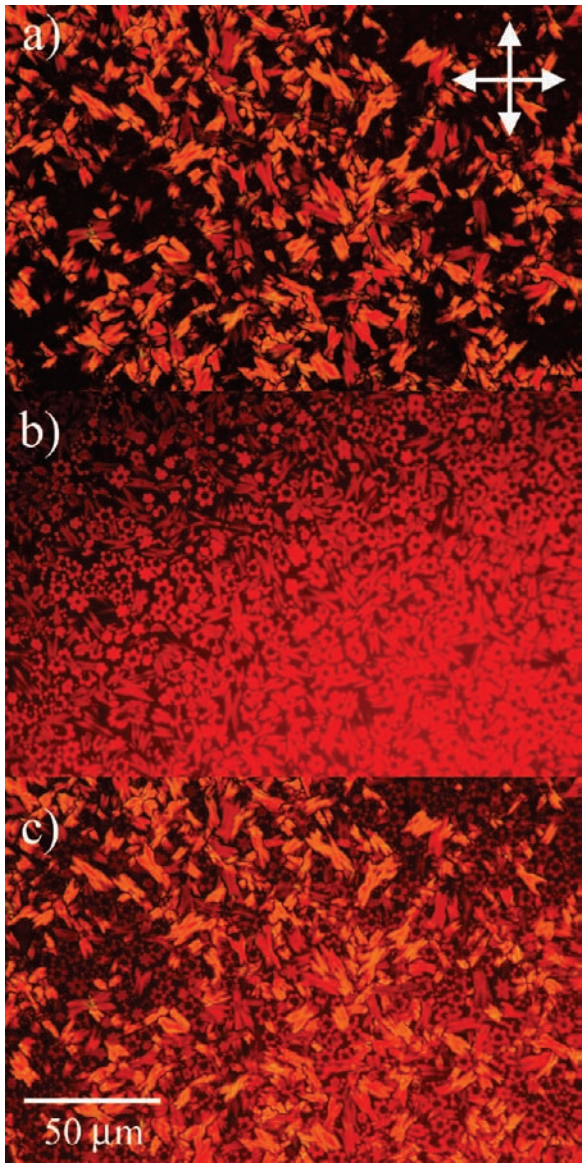


***Figure 10.*** Compound **2** drop-cast on a microscope coverslip and observed by optical microscopy at 194 °C: (a) with a white light in transmission between crossed-polarizers (symbolized by the cross in the corner of the picture) (classical texture); (b) upon irradiation at $300 < \lambda_{ex} < 350$ nm (emission texture without any polarizer); and (c) overlapping of (a) and (b).

perpendicularly to the surface are more emissive than the columns lying on the support surface (chromosome-like elongated motifs). These results demonstrate that, at the molecular scale, the excitation is more efficient when the electromagnetic wave impinges perpendicularly to the pyrene−ethynyl core rather than perpendicularly to the edge of the disk-like molecule. These observations clearly demonstrate that the luminescence properties are not uniform in the mesophase and strongly depend on the orientation of the molecules and aggregates.

## Conclusions

Pyrene substitution with rigid 4-ethynylphenylaminoacyl derivatives provides fluorescent molecules with outstanding features. The double substitution in compound **1** gives rise to low molecular weight gelators, which gelled DMF, toluene, and cyclohexane. The fluorescence is maintained in the gel, and the xerogel is composed of interlocked thin fibers extending over micrometer distances. Intertwining of these molecular chains provide superbundles of larger size. Laser scanning confocal microscopy confirms that the photoluminescence is not dependent on the size of the superstructure of the fiber entanglement and that the 3D architecture efficiently prevents excimer formation. These robust gels were used as the active layer in an organic field-effect transistor. Charge transport across the fiber bundles is very effective without the formation of a charge accumulation layer.

However, the tetrasubstituted pyrene core **2** does not give organo-gelators, but a rather stable liquid crystalline material whose temperature domain ranges from room temperature to 200 °C. Optical microscopy and XRD diffraction confirms the formation a columnar mesophase with a hexagonal symmetry. Textural characterization of the $Col_h$ mesophase was directly observed by luminescence microscopy in the absence of cross-polarizers. Highly fluorescent flower-like motifs having in all cases 6 petals reflect the 6-fold symmetry of the $Col_h$ mesophase.

This remarkable luminescent texture allows one to determine by a simple observation, the size of the domains, the nature of the mesophase and its symmetry, and the molecular orientations that lead to the more efficient luminescence properties. The blue-shift of the emission observed between the mesophase and the isotropic phase (red to orange) is in agreement with the breaking up, at the isotropization point, of large stacks (columns) into smaller stacks made of a few chromophores.

The charge transport and light emission measurements in field-effect configuration demonstrate that bundles of entangled fibers could be used as active material in optoelectronic devices. In particular, it is envisaged that, given the bulky nature of the charge transport, luminescent ethynyl−pyrene gels could be used for the fabrication of OLED-like devices.

**Acknowledgment.** This work was jointly supported by the University of Strasbourg through the European School of Polymer and Materials Chemistry (ECPM) and by the Centre National de la Recherche Scientifique (CNRS) of France. This work was supported at Bologna by EU under project EU-FP6-Marie Curie-035859 (BIMORE) and Grant Agreement Number 248052 (PHOTO-FET) and by Italian Ministry MIUR under Projects FIRB-RBNE033KMA, FIRB-RBIP06JWBH (NODIS), and FIRB RBIPO642YL (LUCI). We thank Dr. C. Bourgogne for the modeling of the liquid crystalline structure, and Dr. Loïc Charbonnière for his help in measuring the fluorescence quantum yields.

**Supporting Information Available:** Complete experimental section including preparation and characterization of the synthetic precursors, DSC traces of compounds **1** and **2**, X-ray crystal data of compound **2** at various temperatures and treatments, solid-state and isotropic state emission for compound **2**, additional SEM micrographs of the DMF xerogels for **1**, and molecular dynamic simulation of the mesophase and molecules packing in the mesophase. This material is available free of charge via the Internet at http://pubs.acs.org.

JA908061Q